RESEARCH PAPER

Efficient transfer and concentration of energy between explosive dual bubbles via time-delayed interactions

C. M. Chang · I. D. Yang · Y. L. Lin ·
C. C. Chieng · F. G. Tseng

Abstract The dynamics of a high heat flux thermal bubble is constrained by the thermal energy carried on the bubble surface right after the bubble formation because of thermal isolation of vapor. This article proposes a way by assigning time delays between dual bubbles to transfer effectively energy from one bubble into the other, thus, breaks energy limitation that one single bubble can usually carry. Experiment result has demonstrated that the useful work as large as 40% can be transferred from one bubble into the other for the ignition time delay set between 2 and 3 μs in a dual bubble system. At the same time, the total extractable useful work in a dual bubble system is 20% higher than twice that of a single-bubble system with the same input heat energy. This phenomenon opens up a new way to transfer or concentrate energies from distributed energy sources with limit energy density into a much higher one for higher power application.

C. M. Chang · Y. L. Lin · C. C. Chieng (✉) · F. G. Tseng (✉)
Institute of Nanoengineering and Micro Systems (NEMS),
National Tsing Hua University, Hsinchu 30013, Taiwan, ROC
e-mail: cchieng@ess.nthu.edu.tw

F. G. Tseng
e-mail: fangang@ess.nthu.edu.tw

C. C. Chieng · F. G. Tseng
Department of Engineering and System Science, National Tsing Hua University, Hsinchu 30013, Taiwan, ROC

F. G. Tseng
Division of Mechanics, Research Center for Applied Sciences Academia Sinica, Taipei 11529, Taiwan, ROC

I. D. Yang
Department of Information Management, China University of Science and Technology, Taipei 11529, Taiwan, ROC

List of symbols

S	Cavity spacing, mm
$\overline{D_b}$	Average bubble departure diameter, mm
D	Separation distance between dual heaters, m
D_s	Half of the maximum bubble size for single heater case, m
MEMS	Micro-electro-mechanical-systems
DT	Ignition time difference of two independently growing bubbles, μs
I	Electrical current, A
r	Resistance of platinum heater, Ω
Area	Heating surface area of the platinum heater, m^2
q''	Heat flux, w/m^2
P_b	Bubble pressure, N/m^2
P_∞	Ambient pressure, N/m^2
R	Bubble radius, m
ρ_l	Density of liquid, kg/m^3
μ_l	Viscosity of liquid, N s/m^2
σ	Surface tension of liquid, N/m
V	Bubble volume, m^3
t_0	Bubble initiating time
$t_{+1/2max}$	The time when bubble grows to half of the maximum bubble volume
t_{max}	The time when volume of the bubble reaches the maximum bubble volume
$t_{-1/2max}$	The time when bubble collapses to half of the maximum bubble volume
$A(t)$	Interfacial surface area, m^2
$W(t)$	Useful mechanical work, J

1 Introduction

The parallel growth/collapse process of explosive micro-thermal bubbles plays an important role in microthermal bubble actuators. The strength of bubble–bubble interactions with various distances and different ignition times between bubbles affects the performance of the actuating systems, such as inkjet printheads (Tseng et al. 2002a, b), peristaltic microbubble pumps (Jun and Kim 1998), and microoptical switches (Uebbing et al. 2006), among others. In the previous literatures, microthermal bubbles have been treated individually as stand-alone energy sources, and the interactions among them have been considered more interference than benefit for performance improvement, such as the cross talk issue in inkjet printheads or optical switches, the time sequencing issue in microbubble pumps, and others. As a result of the stand-alone view of the energy source, very limited energy can be extracted by the heater under high heat flux, constraining a single bubble for higher power generation and actuation. This article provides a different perspective of the time-delayed interactions among bubbles, which can be exploited to extract and concentrate the most possible energy into one bubble from the rest of the bubbles by carefully adjusting their positions and phases. At the same time, cross talk with other bubble systems can be efficiently reduced. In this article, two explosive microbubbles, generated by supplying the same pulse energy but ignited at different instants, are examined to elucidate their dynamic behaviors and the energy transfer between them.

In the literature, many works have been dedicated to understanding bubble dynamics (Akira 1991; Lin et al. 1998; Deng et al. 2003; Hong et al. 2004). In the interaction among multiple bubbles, the growth and re-growth of bubbles can cause adjacent bubbles to collapse rapidly, suppressing the growth of the bubble (Sato et al. 1994). Flow induced by the growth of a bubble can act as a source to suppress the growth of the adjacent bubble (Sato et al. 1994). The ignition delay of the second bubble is demonstrated to be a key parameter that governs bubble–bubble interactions and energy transfer in this study. Among many different bubble interactions, explosive microbubbles have been one of the interests for decades. For example, single-bubble dynamics (Akira 1991; Lin et al. 1998; Deng et al. 2003; Hong et al. 2004) and the effect of interactions on the distance between bubbles have been emphasized. In continuous heating studies, Calka and Judd (1985) studied the interaction phenomena at adjacent nucleation sites (~mm) and concluded that bubble–bubble interactions among nucleation sites could be explained using three zones. They depicted that various non-dimensional cavity spacings, $S/\overline{D_b}$ (cavity spacing over average bubble departure diameter), inhibited bubble formation, promoted bubble

growth, and prevented any bubble from being treatable individually without interaction. Zhang and Shoji (2003) investigated the mechanism of interaction between nucleation sites using two artificial cavities that were separated with different spaces (1–8 mm) and proposed that hydrodynamic interaction, thermal interaction, and coalescences were the three important factors that influenced the interactions between bubbles. These factors compete to promote or suppress bubble departure. Chatpun et al. (2004) arranged three artificial cavities and observed interactions among variously spaced bubbles (1–4 mm). They found that the spacing and pattern arrangements markedly affected the dynamic behavior of the bubbles. Tomita et al. (1990) focused a Q-switch laser (20 ns) to produce bubbles by pulsed heating. They noted that the space (~mm) between the bubbles, their relative sizes, and whether a rigid wall was nearby significantly affected the bubble–bubbles interaction. Yang et al. (2007) supplied a high flux (~GW/m^2) with a pulse width of several microseconds to two microheaters that were separated by a distance ranging from 25 to 125 μm and observed the dynamics of bubble–bubble interactions. When two heaters get closer, depression degree of bubble–bubble interaction is enhanced. As D/D_s (heater spacing over half of the maximum bubble size for single heater) exceeds 5 from the prediction of extrapolated method, no interaction will occur in dual bubble system. Bubble growth/collapse rate can be controlled via heater spacing. Sato et al. (1994) used pulsed laser (30 ns) to generate two bubbles with time difference. The induced source flow and the shock wave emitted from the later bubble led to rapid collapse of the former one during the growth process of the former one. The later bubble deviated original track of Rayleigh bubble due to rebounding motion and a shock wave of the former one during growth of the later bubble. Time difference between two bubbles markedly influenced the bubble–bubble interaction.

From the above literature survey, most of the earlier studies on bubble–bubble interactions have focused on the effects resulting from different bubble–bubble space (Calka and Judd 1985; Zhang and Shoji 2003; Tomita et al. 1990; Yang et al. 2007), arrangement of the nucleation sites (Chatpun et al. 2004), and the presence (or absence) of obstacles (Tomita et al. 1990). However, different ignition times of multiple bubbles are also an important parameter which may greatly affect multiple-bubble dynamics. However, there are still not many articles discussing the energy transfer effect of explosive bubble interactions from different ignition times. Therefore, this study proposes the application of time-delayed ignition of the second bubble to control the interactions and energy transfer between two bubbles. Here, the "delay time" (denoted as "DT") represents the difference between the ignition times of the two

independently growing bubbles. Hopefully through this study, the interaction and energy transfer between dual bubbles can be more understood to open up a new way for bubble manipulation.

2 Experimental methods

2.1 Design

In this study, the maximal size of an individual bubble during the growth/collapse process is chosen as a representative parameter to characterize the degree of bubble enlargement or depression. The snapshots in Fig. 1 captures one bubble's reaching its maximal size during the bubble growth/collapse process and the enhancement or depression of the second ignited bubble (right) by the first (left) bubble with a DT as compared to the maximal size of a single bubble. Different delay times may cause the configuration and size difference of the second bubble from bubble interactions, as shown in Fig. 1. For simultaneous ignitions with a zero delay time (DT = 0 μs), the growth of both bubbles is depressed when they grow simultaneously, so the maximal sizes of the bubbles are smaller than that of an explosive single bubble. When the second bubble is ignited later with DT = 2 μs, the second (right) bubble is apparently larger than that of the single-bubble case. At DT = 2 μs, the collapse of the first ignited (left) bubble acts as a sink which attracts the second ignited (right) bubble to expand. As the delay time is increased to DT = 8 μs, the second (right) bubble is clearly smaller than the single one because of rebound of the first ignited (left) bubble to suppress the growth of the second ignited (right) bubble. In summary, the delay parameter has considerable impact on bubble size. Figure 2 shows a series of four diagrams illustrating the experimental concept. Figure 2a, b indicates the simultaneous application of heating

pulse into the two microheaters without time delay and the corresponding sketch of bubble growth history of each other. Figure 2c, d illustrates the time-delayed application of heating pulses; thus, both of the bubble histories may be changed due to bubble interaction. The bubble evolution images are recorded for further analysis.

2.2 Fabrication process

In this research, bubbles were generated by two microheaters fabricated by the microfabrication technology. Microheaters were made of the platinum film with a heating area of $50 \times 50 \ \mu m^2$ and were located 100 μm apart. Figure 3 reveals the process flow of the microheaters. The detail microheater fabrication is described as follows. First, a 1-μm thermal oxide thin film is grown on the silicon wafer to prevent heat loss into silicon wafer (a). The 300 Å titanium film is then deposited as the adhesion layer for 1,500 Å platinum film coating as the microheater (b), and AZ 5214E photoresist is patterned for Ti/Pt etching (c). After 6,000 Å aluminum film is deposited as the electrode connector (d), AZ 5214E photoresist is patterned for Al etching (e). After 6,000 Å PECVD, the low stress nitride film is deposited as the passivation layer (f), AZ 9260 thick photoresist is patterned for Si_3N_4 etching by reactive ion etching (RIE) to define the windows of wire bond (g). Finally, microheater chip is wire-bonded and packaged (h).

2.3 Experimental setup

2.3.1 Flow visualization system for acquiring high-speed images

Experiments were conducted in a test tank filled with DI water at room temperature. The microbubbles studied in the experiments were produced by applying a constant heat flux 1.2 GW/m² with a pulse width time of 3 μs

Fig. 1 Maximal size of bubbles in bubble–bubble interactions

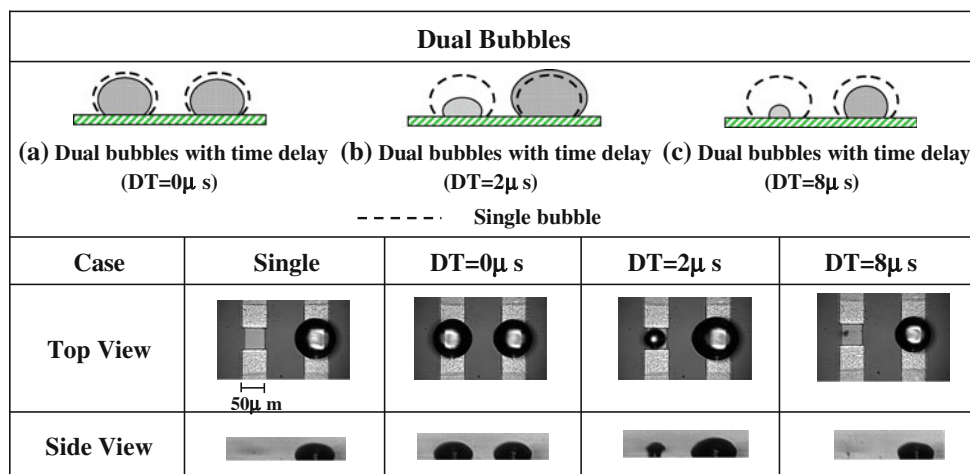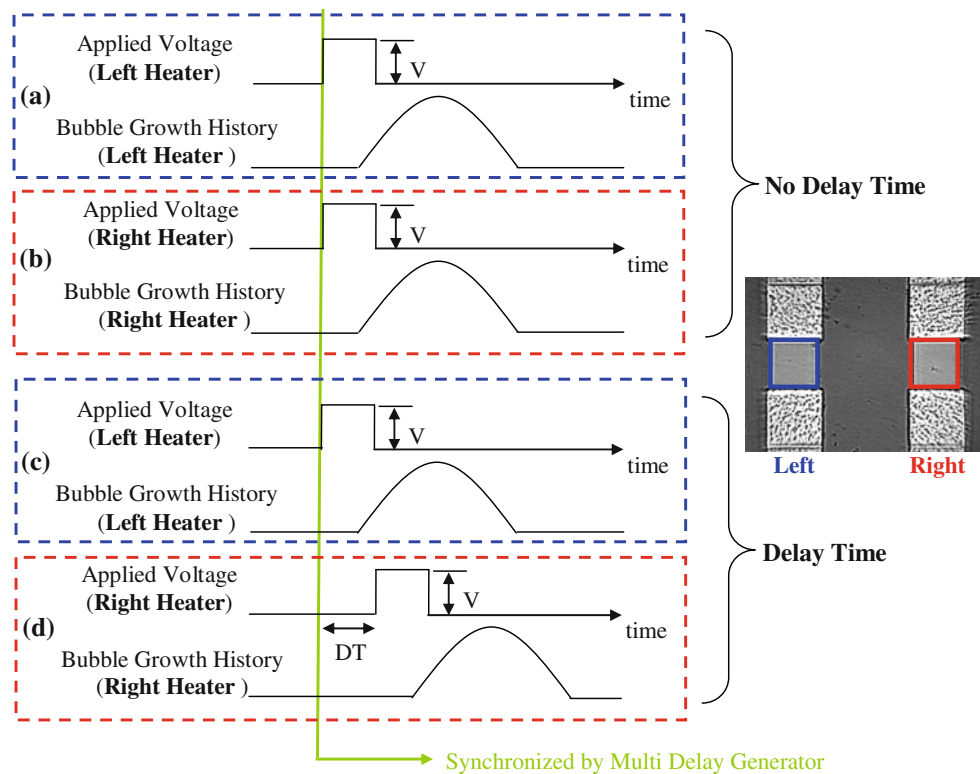|	Dual Bubbles			
	(a) Dual bubbles with time delay (DT=0μ s)	**(b)** Dual bubbles with time delay (DT=2μ s)	**(c)** Dual bubbles with time delay (DT=8μ s)	
	- - - - - Single bubble			
Case	**Single**	**DT=0μ s**	**DT=2μ s**	**DT=8μ s**
Top View	50μ m			
Side View				

Fig. 2 Experimental concept of dual bubble interactions at different time delays

independently at various ignition times. The method for finding the boundary of stable/unstable region of the bubble growth/collapse process was proposed by Lim et al. (2003) to decide the minimum power density for providing ignition current pulse. Longer pulse width would not provide much change on the bubble dynamic. As a result, the pulse width of 3 μs (a little above the stable line) was selected to ensure the stable operation of bubble generation throughout the experiment.

The heat flux of the heater can be described by the following equation:

$$q'' = \frac{I^2 \cdot r}{\text{Area}} \tag{1}$$

where q'' is the heat flux, I is the current of the circuit, r is the sheet resistance of the platinum heater, and Area is the surface area of the platinum heater.

According to Eq. 1, the heat flux is fixed to 1.2 GW/m² for all different cases throughout this research.

In order to illuminate the flow field, two 60 W xenon flash lamps (Hamamatsu Inc., xenon flash lamp, Japan) were employed as the stroboscopes and triggered by pulse signals. The frame rate and exposure time of two high-resolution cooled CCDs (COOKE Inc., USA) was set to 8 frames/s and 500 ns, respectively, to freeze the bubble dynamic image. Top views and side views of the bubble evolution process were captured simultaneously. A

multichannel delay generator (BNC, Model 555, USA) was employed as a synchronizer for triggering the stroboscopes, CCDs, and heating pulses. The multichannel delay generator controlled the bubble ignition times independently for the bubbles. The system setup is illustrated in Fig. 4. Due to the limitation of flashing rate of strobescope and the frame rate (8 frames/s) of the CCD camera, life time of a microbubble is too short (∼10 μs) to be observed directly. As a result, the phase average method was employed to acquire the bubble dynamic images. The phase average method is a technology based on the occurrence of repeating events and statistical approach to record the histories of bubble growth and collapse process. The operation method contains cycles of events as illustrated in Fig. 5. For Event 1, when $t = t_1$, three steps are performed, including (a) 3 μs heating pulse is generated by a constant voltage applied to the microheater, (b) a thermal microbubble is generated with a time delay, and (c) image is captured at phase 1 with a designated time which is t_1 delay to that of the pulse ignition (the gating time was 500 ns). By adjusting different time delays, as t_1, t_2, t_N..., different phases of bubble growth are recorded. The operation frequency in the experiments is estimated as 1 Hz. Figure 5b shows the bubble growth/collapse process using the phase average technique. In this study, six images are taken for each phase (t_N) to meet the statistical requirement.
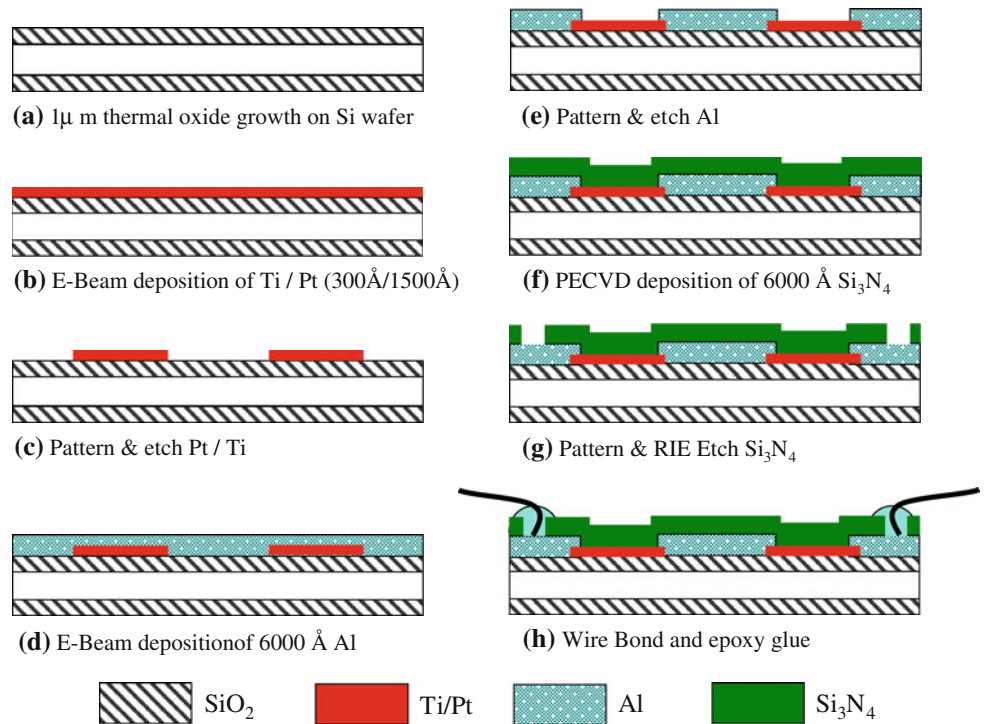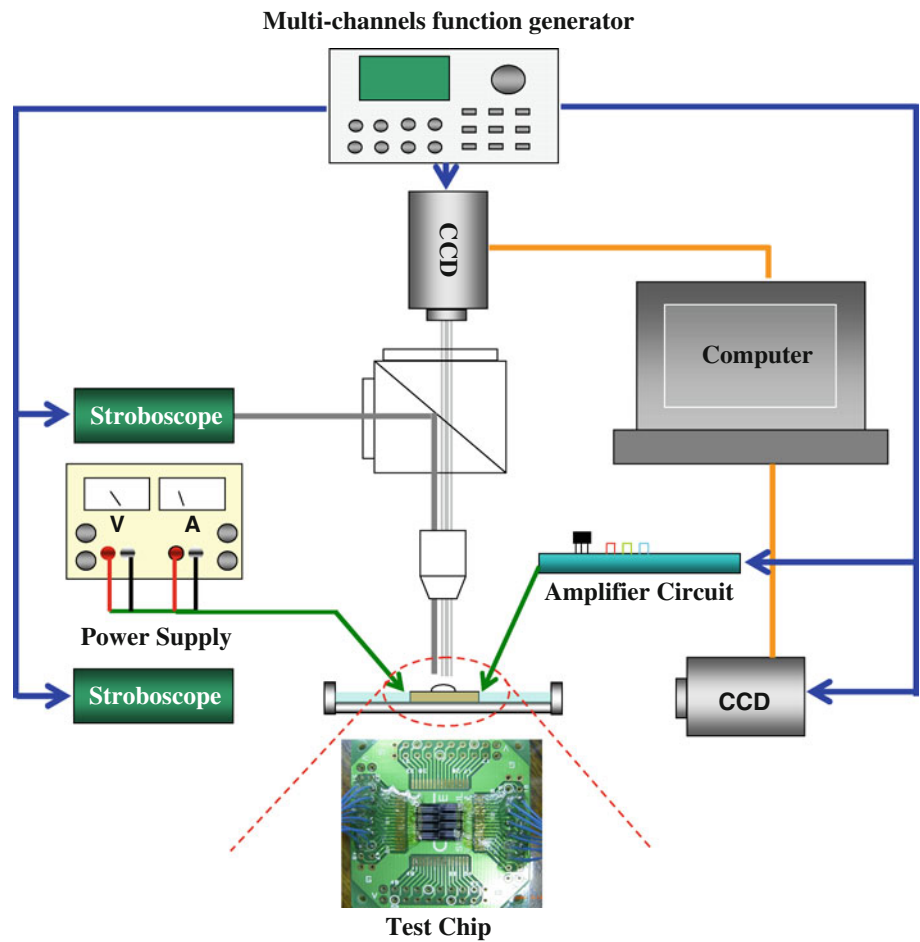
Fig. 3 Fabrication process of microheater

(a) 1μ m thermal oxide growth on Si wafer

(b) E-Beam deposition of Ti / Pt (300Å/1500Å)

(c) Pattern & etch Pt / Ti

(d) E-Beam depositionof 6000 Å Al

(e) Pattern & etch Al

(f) PECVD deposition of 6000 Å Si_3N_4

(g) Pattern & RIE Etch Si_3N_4

(h) Wire Bond and epoxy glue

SiO_2 Ti/Pt   Al Si_3N_4

Fig. 4 Setup of flow visualization system

Multi-channels function generator

CCD

Stroboscope

Computer

V   A

Amplifier Circuit

Power Supply

Stroboscope

CCD

Test Chip
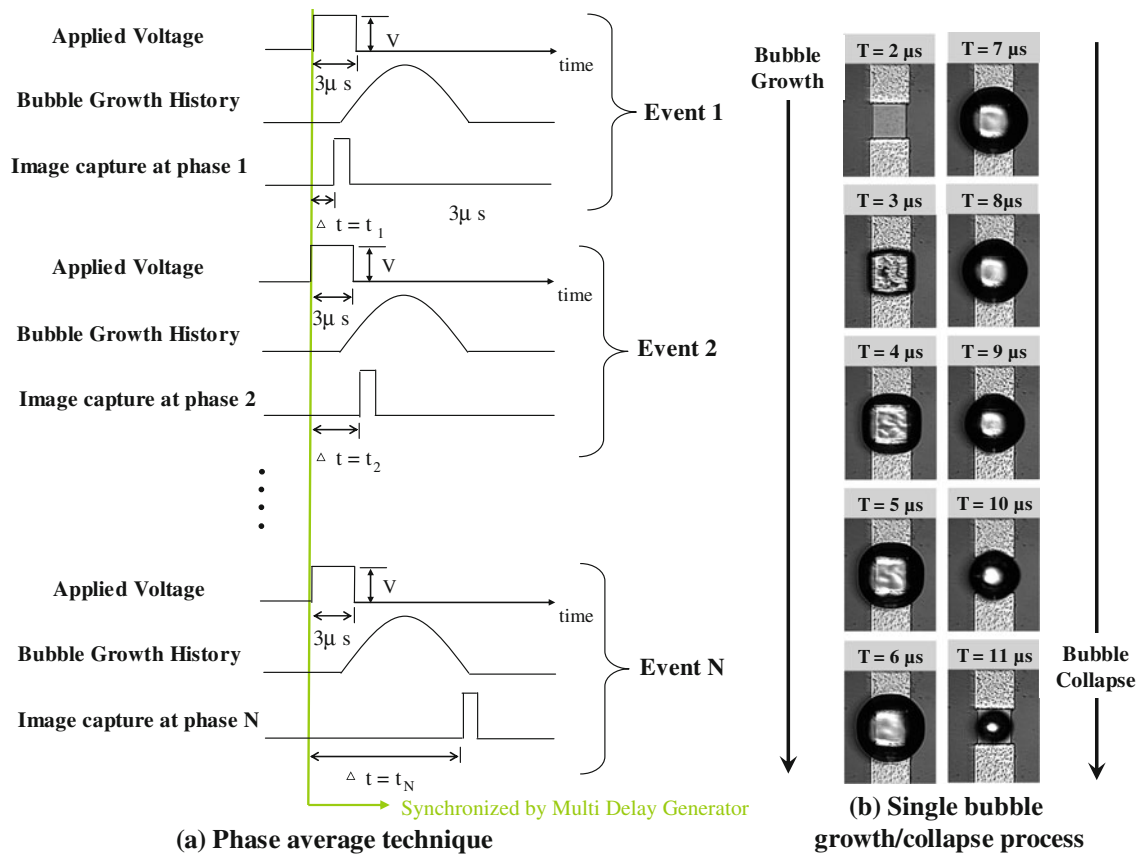
Fig. 5 Principle of phase average method process

2.3.2 Flow visualization system setup for μPIV

Particle image velocimetry in microscale flow field (μPIV) is a very useful tool for flow field measurement in the current study. The apparatus of μPIV system is sketched in Fig. 6. The μPIV system (TSI Inc., PIV system, USA) utilizes the Nd–YAG laser to illuminate the fluorescent particles to record the particle images within a time interval 0.6 μs. Polystyrene particles tagged with fluorescence dye are of diameter 1 μm and specific gravity of $\rho = 1.055$ and applied for flow field tracking. $20\times$ objective lens (Olympus, Japan) with $NA = 0.4$ was employed for PIV images and the spatial resolution of the velocity field related to the interrogation spot size and the measurement depth is estimated as 16.9 μm. Those particles absorb green light at $\lambda = 532$ nm and emit red light at $\lambda = 612$ nm. The recorded images pairs are analyzed by a software (INSIGHT[TM] and TECPLOT, USA) to obtain the flow field. The images at different phases with time steps of 1 μs are recorded for quantitative analysis. The maximum velocity measured in this study is about 4.5 m/s.

3 Results and discussion

3.1 Evolution of single bubble

Figure 7 defines x, y, and z directions of bubble extensions at DT = 0 in Fig 7a and b from top view and side view, respectively. A specified grayscale value of the image edge was first set for determining the bubble boundary and region of interest (ROI). The top view and side view images were acquired at a resolution of 0.71 and 1.11 μm/pixel, respectively. The volume of a bubble was obtained by integrating through the bubble topography rebuilt from the top/side view images. Six images at the same bubble evolution phase but different bubble cycle were averaged to obtain the final volume value. The small deviation (<5%) of the data indicated good repeatability of the bubble evolution cycle and accuracy of the experiments.

In this experiment, the same constant heat flux and pulse width are applied to all heaters but the ignition time is different. By adjusting the ignition time differently, mutual interaction behaviors of bubbles can be obtained. In order to ensure experimental accuracy and stability of the

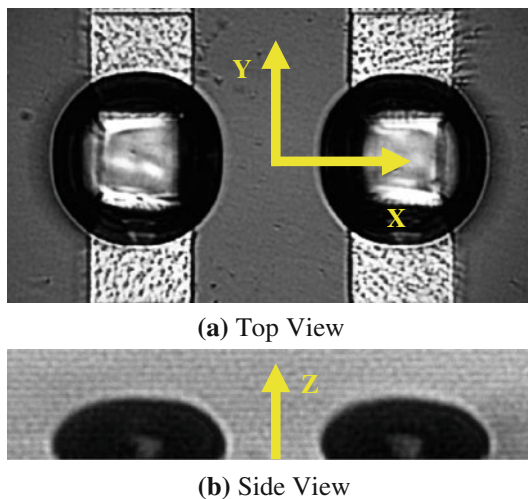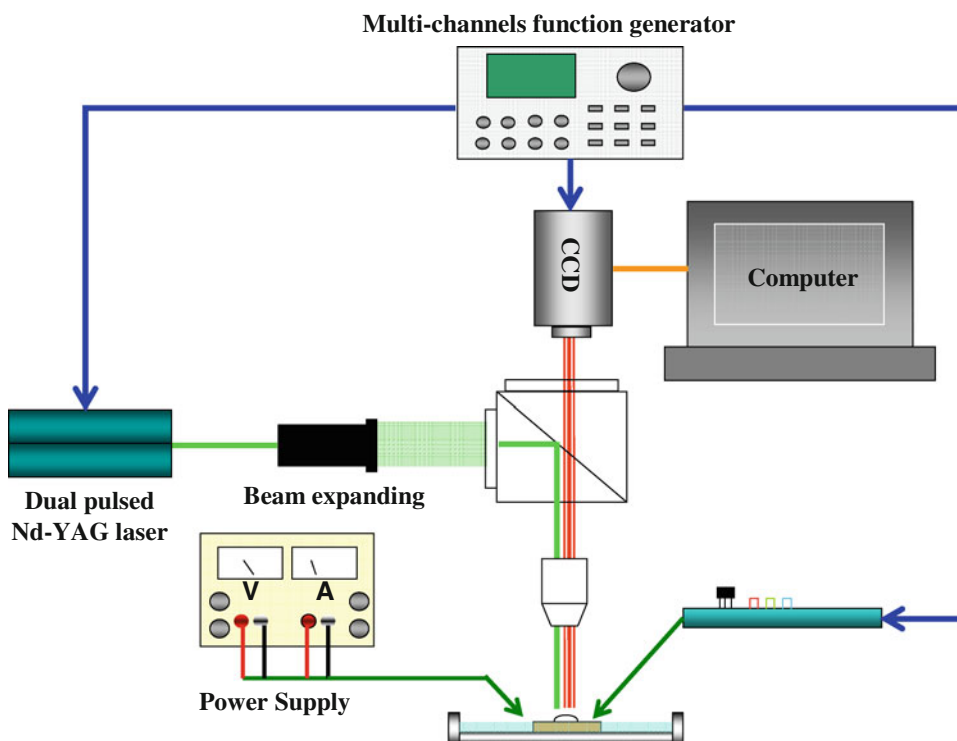**Fig. 6** Setup of the microparticle image velocimetry system

(a) Top View

(b) Side View

Fig. 7 Definitions of x, y, and z direction for dual bubble system

heaters, the growth/collapse histories of the left and right bubbles are recorded and compared separately in two cross sections (Fig. 8, single bubble). A vapor sheets are observed on single left/right heaters at 2.2 μs after the heater ignition [Fig. 8, single bubble (a)]. After 2.2 μs, the bubble keeps growing and reaches a maximum size at 7 μs [Fig. 8, single bubble (c)]. In the mean time, bubble is changed from square [Fig. 8, single bubble (a)] into circular shape [Fig. 8, single bubble (c)] during growth process. In Fig. 8, single bubble case, (d)–(f), illustrate that bubble shrinks toward the center of heater during bubble

collapsing process. Figure 9a plots the histories of the bubble diameters in three dimensions and the estimated bubble volume of the single bubble.

Due to the complexity in bubble dynamic interaction when it encounters a solid wall, Zhao et al. (2000) assume that the bubble radius obtained by Eq. 2 represents the characteristic length of the bubble volume to calculate the vapor pressure ($P_b(t)$) by using Rayleigh–Plesset equation:

$$P_b(t) - P_\infty = \rho_l R \frac{d^2 R}{dt^2} + \frac{3}{2}\rho_l \left(\frac{dR}{dt}\right)^2 + \frac{4\mu_l}{R}\frac{dR}{dt} + \frac{2\sigma}{R} \quad (2)$$

where $P_b(t)$ is the bubble pressure, P_∞ is the atmospheric pressure (101.3 kPa), R is the bubble radius, and ρ_l, μ_l, and σ are liquid density, liquid viscosity, and liquid surface tension, respectively. For water, the properties at the boiling point are used as $\rho_l = 958$ kg/m^3, $\mu_l = 2.83 \times 10^{-4}$ N s/m^2, and $\sigma = 0.0589$ N/m, at 100°C.

Since the bubble is assumed as a sphere in deriving Rayleigh equation, the bubble radius (R) can be related to bubble volume ($V(t)$) by

$$R(t) = \left(\frac{3V(t)}{4\pi}\right)^{1/3} \quad (3)$$

From the pressure obtained by Eq. (2), pressure peaks occur as a bubble starts to grow. The same growth histories/pressure peaks in Fig. 9a are shown for both left and right bubbles, and the coincidence indicates that the initial conditions and behaviors are the same.
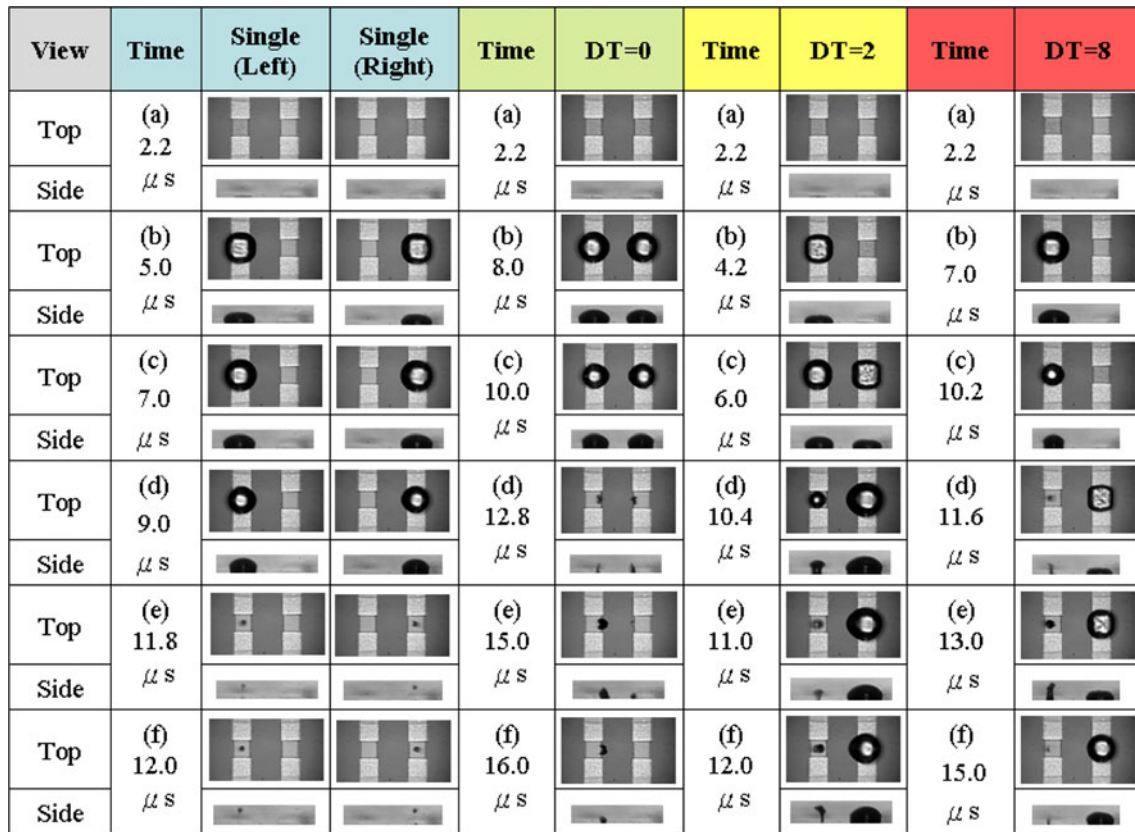
Fig. 8 The snapshot images of growth and collapse process of single bubble, dual bubble at DT = 0, DT = 2, and DT = 8, respectively

3.2 Interactions of dual bubbles

3.2.1 DT = 0

Figure 8 (DT = 0) plots the histories of bubble shape/size evolution for DT = 0 μs. Dual bubbles are ignited simultaneously, and the vapor sheets are observed at 2.2 μs after the heating starts [Fig. 8, DT = 0(a)]. The bubbles continue expanding and reach the maximum at 8.0 μs [Fig. 8, DT = 0(b)]. Because dual bubbles are generated simultaneously with a pressure peak applied on each other mutually (Fig. 9b, DT = 0 μs), they depress each other and result in a smaller size of the bubbles than that of the single-bubble case. For the collapsing process, bubbles are attracted each other and the bubbles appear hemispherical shapes from top-view images [Fig. 8, DT = 0 (b), (c)]. At the end of collapsing process [Fig. 8, DT = 0 (d), (f)], bubbles are re-expanded and the process is called rebound process. In our previous work (Yang et al. 2006), two possible explanations of this phenomenon have been raised, including: (1) implosion mechanism of cavitation whereby extremely high pressure are produced with compression wave, and (2) violent collapsing of a gas bubble in the liquid overshoots its equilibrium size and regrows many times.

Figure 10 (DT = 0) shows the velocity fields during bubble growth/collapse processes at the cutting plane at $Z = 16$ μm for DT = 0 case. Velocity fields are represented by magnitude contours in colors and directions in vectors at four characteristic times, i.e., the time bubble starts to grow (t_0), the time the bubble reaches the size of half maximum ($t_{+1/2max}$), the time the bubble size reaches the maximum (t_{max}), and the time bubble collapses into the size of half maximum ($t_{-1/2max}$). Because of zero delay between the dual bubbles, the obtained velocity fields are symmetrical at these characteristic times.

3.2.2 DT = 2

Figure 8 (DT = 2) depicts the snapshot images of growth, collapse, and rebound process for DT = 2 μs, measured at different time instants. The second (right) bubble is ignited with 2 μs delay to the ignition time of the first (left) bubble and the second bubble is ignited during the expansion period of the first one [right; Fig. 8, DT = 2 (b)]. When the second (right) bubble is ignited, the pressure exerted by the second (right) bubble is the most possible cause affecting the growth of the first (left) bubble and then the growth rate is slowing down and slower than that in the single-bubble case (Fig. 9c, DT = 2 μs). As the first bubble begins to
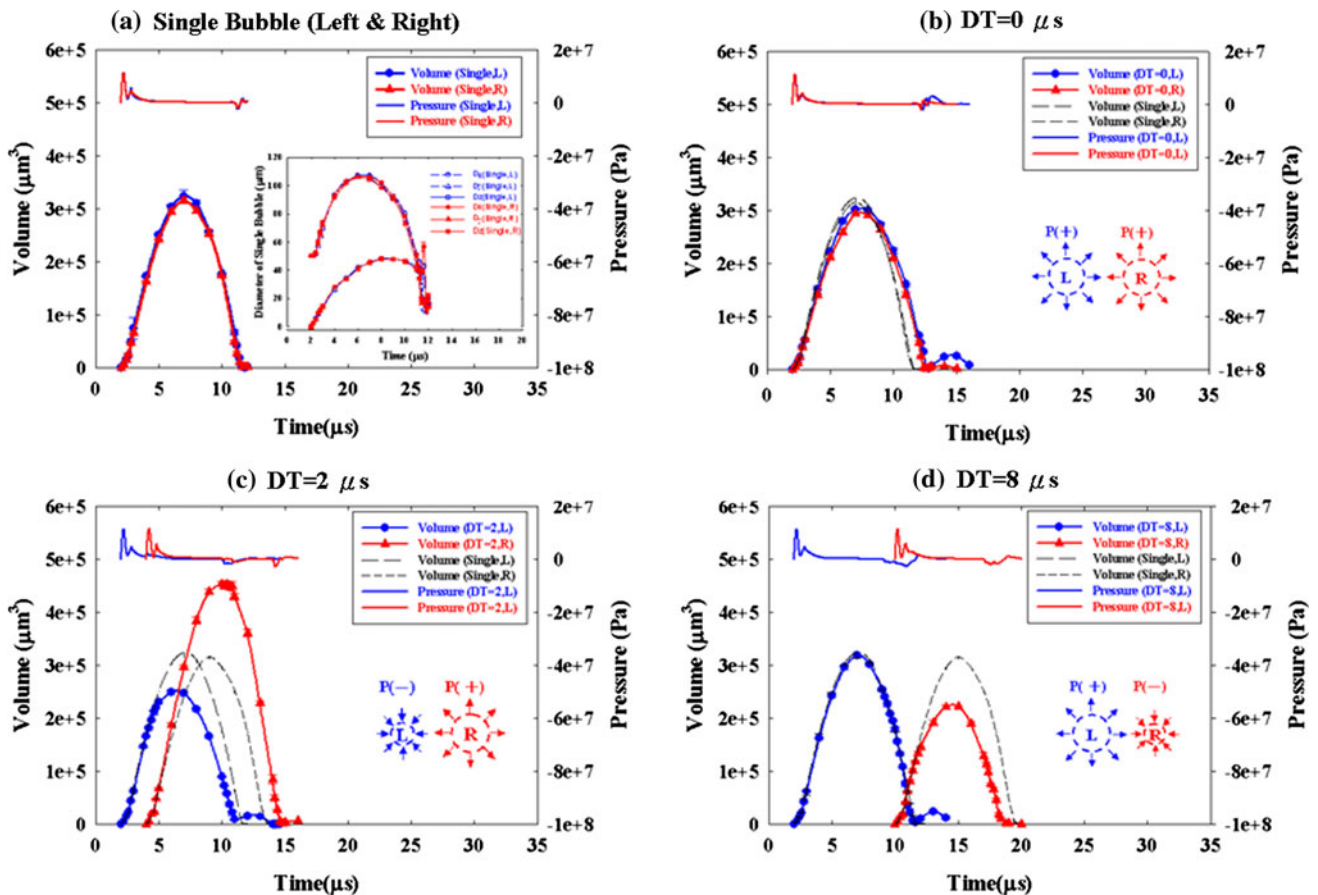
Fig. 9 The histories of measured bubble volume and the corresponding bubble pressure for dual bubbles cases of **a** single bubble, **b** DT = 0 μs, **c** DT = 2 μs, and **d** DT = 8 μs

collapse, the fluid that surrounds the first bubble acts as a sink [Fig. 10, DT = 2 μs (c)] and promotes the growth of the second (right) bubble. Figure 8 [DT = 2 (d), (e)] shows that the growth of the second bubble is attracted by the first one. Therefore, the second (right) bubble grows larger than the first bubble. When the first bubble rebounds, it produces a small peak pressure in Fig. 9c. The peak pressure promotes the rapid collapse of the second bubble.

3.2.3 DT = 8

Figure 8 (DT = 8) depicts the snapshot images of the growth, collapse, and rebound process for DT = 8 μs, measured at different time instants, and Fig. 9d plots the histories of bubble volumes and the corresponding pressures. The volume of the second (right) bubble follows the volume history in the single-bubble case until the first (left) bubble rebounds. The rebound of the first (left) bubble with the corresponding source-type flow and peak pressure limits the growth of the second (right) bubble and the

maximal size of second bubble is smaller than that of the single bubble.

However, in this study, the rebound process undergoing a time delay induces a very different effect on the restriction of the second bubble growth when the rebound bubble initiates at the rising/collapsing period of the second bubble. As a result, the rising curve of the second bubble will be stopped when the rebound bubble ignites in the mean time, as shown in Fig. 9d. On the other hand, the falling slop of the second bubble will become steeper when the rebound bubble starts growing at the collapsing period of the second bubble, as shown in Fig. 9c. The second bubble growth is truncated short no matter which situation is encountered. This phenomenon may be useful to help on the termination of the second bubble in a shorter time for the next cycle of bubble generation.

In summary, the bubble growing/collapsing process are affected by the growing/collapsing of the nearby microbubble in terms of the induced flow field and the bubble pressure peak for different delay times.
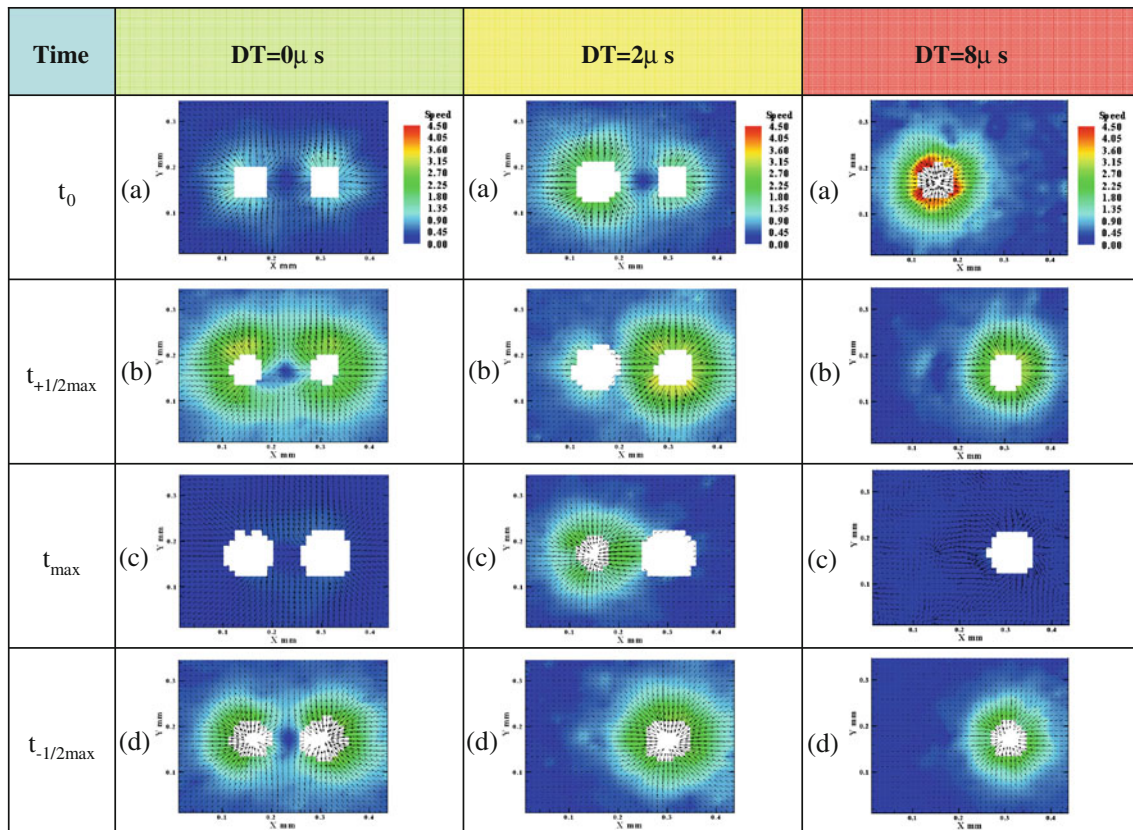
Fig. 10 µPIV measurements of the induced flow velocity fields by dual bubbles at the cutting plane Z = 16 µm for DT = 0 µs, DT = 2, and DT = 8

3.3 Normalized maximum bubble volume versus delay time

Figure 11 plots the maximal bubble sizes versus delay time for explosive dual bubbles. The maximal size of each bubble during the growth/collapse process is normalized by the maximal size of a single explosive bubble. The maximal size of the bubbles is slightly smaller than that in the single-bubble system, if all bubbles are ignited at the same time (DT = 0 µs). As DT increases, the maximal size of the second (right) bubble gradually rises to its highest value at DT = 2 µs (given a range of delays from 0 to 10 µs). For DT = 2 µs, the maximum volume of the first bubble is 20% smaller than that of a single bubble and the volume of the second (right) bubble is approximately 40% larger than that of a single bubble. Moreover, the maximal size of the first bubble recovers that of the single bubble when DT exceeds 5 µs. The effect of the second (right) bubble on the first one is small for DT larger than 5 µs. For DT = 8 µs, the size of the first (left) bubble remains that of the single bubble, whereas the volume of the second (right) bubble is 30% smaller than the single bubble because the re-growth of the first bubble produces a pressure peak that suppresses the growth of the second bubble. When the delay time is increased larger than 10 µs, the bubbles have no effect on each other. The observations verify that the delay is an effective parameter in controlling the enhancement or depression of the growth of bubbles.
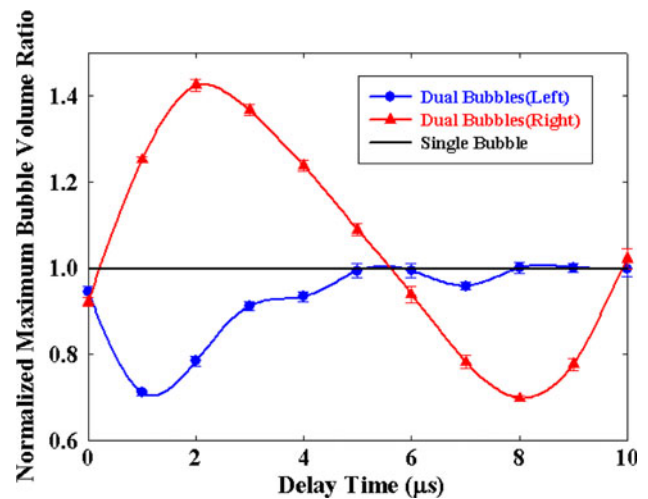

Fig. 11 Normalized maximum bubble volume ratio versus delay time

3.4 Useful energy under different delay times

In addition, a bubble–bubble interaction can be characterized in terms of useful energy transfer between bubbles. The useful work for the bubble system can be expressed as (Zhao et al. 2000)

$$W(t) = p_b\, V(t) - p_\infty\, V(t) - \sigma A(t) \qquad (4)$$

which is the net energy after the ambient and interface energy of vapor/liquid has been overcome. The calculated useful work for each of the bubble is shown in Fig. 12. The similarity between Figs. 11 and 12 reveals that bubble expansion/contraction is correlated to the useful work of the corresponding bubble for various time delays. There is a slight useful work decrease at DT = 0 μs in Fig. 12. Since the two bubbles are ignited simultaneously, the dynamics and flow field of them are symmetrical in the growth/collapse process [Figs. 8, DT = 0 (a)–(d), 10, DT = 0] that is one bubble is a mirror bubble of the other. The coexistence of the mirror bubble, as a result, will depress each other to hinder energy transfer from heat into a useful work. With increasing DT, the useful work of the second (right) bubble rises gently and reaches maximum in the range of DT = 2–3 μs. For the two bubble system compared to the single-bubble system, useful work as large as 40% can be transferred from one bubble into the other between DT = 2 and DT = 3 μs. During this time period, the second (right) bubble expands outward at the rising period and the first (left) bubble collapses inward at the same time. The collapse of the first bubble behaves like a sink to help the second bubble expand and grow effectively. As a result, the total useful work reaches the maximum by adding the works of the two bubbles together at DT between 2 and 3 μs, which means a highest energy transfer efficiency occurs from heat energy into the useful work (the input heat energy is kept the same for all cases)
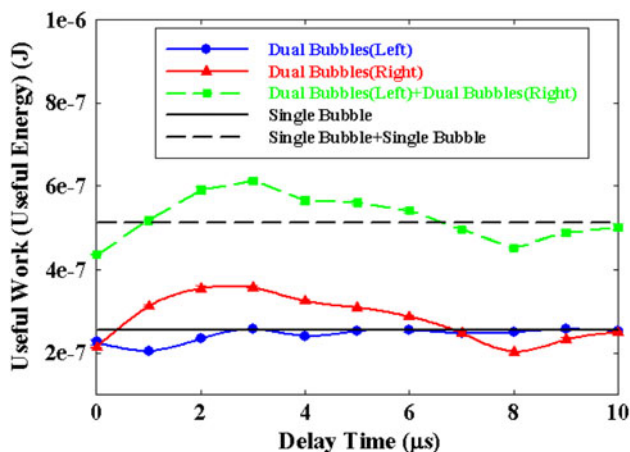

Fig. 12 Useful work calculated for different bubble delay time

at this time period. After DT = 3 μs, the useful work curve of the second bubble starts to decline, reaches the lowest level at DT = 8 μs, and then returns to that of the single-bubble level at DT = 10 μs. The rebound process has the highest effect at DT = 8 μs which greatly restrict the growth of the second bubble; thus, the lowest useful work is obtained for the second bubble. The total useful work by summing the energies of the first and second bubbles is calculated under different time delays, as shown in Fig. 12, the curve of Dual Bubbles (left) + Dual Bubbles (right). It is clear that the total useful work of the dual bubble systems is larger than twice that of the single bubble for DT from 2 to 6 μs, indicating higher energy transfer efficiencies appearing in this region. Among them, DT between 2 and 3 μs provides the highest useful work, which is 20% higher than twice that of the single-bubble system. Therefore, by proper design of the ignition times, most of the heat energy supplied into the bubble system can be efficiently extracted and concentrated into one bubble, which can be useful to break the energy limitation of a stand-alone single bubble for higher energy applications. In this experiment, when the time delay is between 2 and 3 μs, it offers an optimized energy transfer point with highest useful work and energy transfer efficiency.

4 Conclusion

In this study, delay times of explosive dual microbubbles are controlled precisely to understand the complex and dynamic phenomenon of dual bubbles interactions. The interactions have been characterized in terms of maximal bubble size, sink/source flow, bubble pressure, and useful work. For DT = 0 μs, dual bubbles are produced simultaneously, and the produced pressures inhibit the growth of each other. The sizes of those are slightly smaller than that of a single bubble. For DT = 2 μs, the pressure generated from the second (right) bubble affects the growth of the first (left) bubble in the beginning and poses the first bubble growth slower than the single bubble. When the first (left) bubble starts to collapse, the surrounding flow field induces a sink flow to promote the growth of the second (right) bubble. As the first (left) bubble rebounds, the peak pressure produced by the rebound leads to a rapid collapse of the second (right) bubble. For DT = 8 μs, the first (right) bubble keeps following the history of the single bubble because there is no influence from the second (right) one. As the first bubble rebounds in the same condition, the volume history of the second bubble drops and deviates from the original track of the single bubble. For the volume variation, at DT = 2 μs, the volume of the first bubble is 20% smaller than that of a single bubble, whereas the volume of the second (right) bubble is approximately 40%

larger than that of a single bubble, which provides a maximum volume difference between two bubbles. At the similar time delay for DT = 2–3 μs, the total useful work reaches a maximum which is 20% higher than twice that of the single-bubble system under the same heat energy input. This also indicates the optimized operation point with highest energy transfer efficiency. In summary, when the time delay is between 2 and 3 μs, the dual bubble system offers optimized operation parameters with highest useful work and energy transfer efficiency.

References

Akira A (1991) Bubble dynamics in boiling under high heat flux pulse heating. ASME J Heat Transf 113:973–979

Calka A, Judd RL (1985) Some aspects of the interactions among nucleation sites during saturated nucleate boiling. Int J Heat Mass Transf 28:2331–2342

Chatpun S, Watanabe M, Shoji M (2004) Experimental study on characteristics of nucleate pool boiling by the effects of cavity arrangement. Exp Therm Fluid Sci 29:33–40

Deng P, Lee YK, Cheng P (2003) The growth and collapse of a micro bubble under pulse heating. Int J Heat Mass Transf 46:4041–4050

Hong Y, Ashgriz N, Andrews J (2004) Experimental study of bubble dynamics on a micro heater induced by pulse heating. ASME J Heat Transf 126:259–271

Jun TK, Kim CJ (1998) Valveless pumping using traversing vapor bubbles in microchannels. J Appl Phys 83:5658–5664

Lim JH, Lee YS, Lim HT, Baek SS, Kuk K, Oh YS (2003) Visualization of bubbles generated by micro heaters with various current density distributions. In: Proceedings of the 16th annual international conference of IEEE on micro electro mechanical systems, Kyoto, Japan, Jan 2003, pp 197–200

Lin L, Pisano AP, Carey VP (1998) Thermal bubble formations on polysilicon micro resistors. ASME J Heat Transf 120:735–742

Sato K, Tomita Y, Shima A (1994) Interaction of two bubbles produced with time difference. In: ASME fluids engineering division summer meeting cavitation and multiphase flow, vol 194, New York, USA, pp 1–5

Tomita Y, Shima A, Sato K (1990) Dynamic behavior of two-laser-induced bubble in water. Appl Phys Lett 57:234–236

Tseng FG, Kim CJ, Ho CM (2002a) A high-resolution high-frequency monolithic top-shooting microinjector free of satellite drops—Part I: concept, design, and model. J Microelectromech Syst 11:427–436

Tseng FG, Kim CJ, Ho CM (2002b) A high-resolution high-frequency monolithic top-shooting microinjector free of satellite drops—Part II: fabrication, implementation, and characterization. J Microelectromech Syst 11:437–447

Uebbing JJ, Hengstler S, Schroeder D, Venkatesh S, Haven R (2006) Heat and fluid flow in an optical switch bubble. J Microelectromech Syst 15:1528–1539

Yang ID, Tseng FG, Chang CM, Chieng CC (2006) Microbubble formation dynamics under high heat flux on heaters with different aspect ratios. Nanoscale Microscale Thermophys Eng 10:1–28

Yang ID, Tseng FG, Yu RJ, Chieng CC (2007) Bubble dynamics for explosive microthermal dual bubbles. J Microelectromech Syst 16:734–745

Zhang L, Shoji M (2003) Nucleation site interaction in pool boiling on the artificial surface. Int J Heat Mass Transf 46:513–522

Zhao Z, Glod S, Poulikakos D (2000) Pressure and power generation during explosive vaporization on a thin-film micro heater. Int J Heat Mass Transf 43:281–296